



Encephalitic Alphaviruses Exploit Caveola-Mediated Transcytosis at the Blood-Brain Barrier for Central Nervous System Entry

Hamid Salimi,^a Matthew D. Cain,^a Xiaoping Jiang,^a Robyn A. Roth,^a Wandy L. Beatty,^a Chengqun Sun,^b William B. Klimstra,^b Jianghui Hou,^a Robyn S. Klein^{a,c,d}

^aDepartment of Medicine, Washington University School of Medicine, St. Louis, Missouri, USA

^bDepartment of Immunology and Center for Vaccine Research, University of Pittsburgh, Pittsburgh, Pennsylvania, USA

^cDepartment of Pathology & Immunology, Washington University School of Medicine, St. Louis, Missouri, USA

^dDepartment of Neuroscience, Washington University School of Medicine, St. Louis, Missouri, USA

ABSTRACT Venezuelan and western equine encephalitis viruses (VEEV and WEEV, respectively) invade the central nervous system (CNS) early during infection, via neuronal and hematogenous routes. While viral replication mediates host shutoff, including expression of type I interferons (IFN), few studies have addressed how alphaviruses gain access to the CNS during established infection or the mechanisms of viral crossing at the blood-brain barrier (BBB). Here, we show that hematogenous dissemination of VEEV and WEEV into the CNS occurs via caveolin-1 (Cav-1)-mediated transcytosis (Cav-MT) across an intact BBB, which is impeded by IFN and inhibitors of RhoA GTPase. Use of reporter and nonreplicative strains also demonstrates that IFN signaling mediates viral restriction within cells comprising the neurovascular unit (NVU), differentially rendering brain endothelial cells, pericytes, and astrocytes permissive to viral replication. Transmission and immunoelectron microscopy revealed early events in virus internalization and Cav-1 association within brain endothelial cells. Cav-1-deficient mice exhibit diminished CNS VEEV and WEEV titers during early infection, whereas viral burdens in peripheral tissues remained unchanged. Our findings show that alphaviruses exploit Cav-MT to enter the CNS and that IFN differentially restricts this process at the BBB.

IMPORTANCE VEEV, WEEV, and eastern equine encephalitis virus (EEEV) are emerging infectious diseases in the Americas, and they have caused several major outbreaks in the human and horse population during the past few decades. Shortly after infection, these viruses can infect the CNS, resulting in severe long-term neurological deficits or death. Neuroinvasion has been associated with virus entry into the CNS directly from the bloodstream; however, the underlying molecular mechanisms have remained largely unknown. Here, we demonstrate that following peripheral infection alphavirus augments vesicular formation/trafficking at the BBB and utilizes Cav-MT to cross an intact BBB, a process regulated by activators of Rho GTPases within brain endothelium. *In vivo* examination of early viral entry in Cav-1-deficient mice revealed significantly lower viral burdens in the brain than in similarly infected wild-type animals. These studies identify a potentially targetable pathway to limit neuroinvasion by alphaviruses.

KEYWORDS IFNAR, Venezuelan encephalitis virus, western equine encephalitis virus, alphavirus, blood-brain barrier, caveola-mediated transcytosis, caveolin-1, *in vivo* animal model, transcytosis assay, type I interferon

The central nervous system (CNS) is protected from pathogens by the blood-brain barrier (BBB), an intercellular association of transmembrane junctional proteins between brain microvascular endothelial cells (BMECs), with associated pericytes, as-

Citation Salimi H, Cain MD, Jiang X, Roth RA, Beatty WL, Sun C, Klimstra WB, Hou J, Klein RS. 2020. Encephalitic alphaviruses exploit caveola-mediated transcytosis at the blood-brain barrier for central nervous system entry. *mBio* 11:e02731-19. <https://doi.org/10.1128/mBio.02731-19>.

Editor Nisha K. Duggal, CDC

Copyright © 2020 Salimi et al. This is an open-access article distributed under the terms of the [Creative Commons Attribution 4.0 International license](https://creativecommons.org/licenses/by/4.0/).

Address correspondence to Robyn S. Klein, rklein@wustl.edu.

Received 12 October 2019

Accepted 23 December 2019

Published 11 February 2020

trocytes, and neurons that together comprise the neurovascular unit (NVU) (1). Neurotropic pathogens have evolved mechanisms to bypass or cross this barrier, including anterograde or retrograde transport along axons, destabilization of BBB junctional proteins, or passage through BMECs (2), the last of which may involve intracellular transport within leukocytes via binding to intercellular adhesion molecule 1 (ICAM-1) (3). An additional mechanism may involve caveolae, flask-shaped plasma membrane invaginations within BMECs that are important for cell metabolism, signal transduction, and the transcytosis of large proteins (4). BBB formation of caveolae, which contain the major structural protein caveolin-1 (Cav-1), is limited by the major facilitator superfamily domain-containing protein 2a (Mfsd2a), which is exclusively expressed on BMECs and induced by pericytes (5). Stabilization of junctional proteins and caveolae within BMECs is additionally regulated by the small Rho GTPases, including the Ras homolog gene family, member A (RhoA), and Ras-related C3 botulinum toxin substrate 1 (Rac-1) (6). While many viruses have evolved to interact with Rho GTPases to increase their entry and replication within target cells (7, 8), some neurotropic viruses, including retroviruses and flaviviruses, may compromise BBB permeability via GTPase-mediated alterations of junctional proteins (9–12). For these viruses, neuroinvasion coincides with BBB instability. In contrast, encephalitic alphaviruses, including Venezuelan, western, and eastern equine encephalitis viruses (VEEV, WEEV, and EEEV, respectively), can enter the CNS directly from the bloodstream via unknown mechanisms (13, 14).

VEEV, WEEV, and EEEV naturally cycle between mosquitoes and birds (EEEV and WEEV), mosquitoes and rodents (VEEV enzootic cycle), or mosquitoes and horses (VEEV epizootic cycle) and are all widely distributed in North, Central, and South America (15). Human infection can progress rapidly to encephalitis with fatality rates of 1 to 75%, depending on the strain. Of the three, VEEV is considered the most important zoonotic pathogen, with several reported outbreaks in South and Central America, the latter of which have spread to North America. Although the number of human cases reported is small, the possibility for disease emergence is high due to expansion and spread of mosquito vectors (16). Despite the epidemic potential of VEEV and the high morbidity and/or case fatality rates of EEEV and WEEV, there are no approved vaccines or therapeutics for humans. Insight into the cell-intrinsic and cell-extrinsic processes by which the host limits alphavirus infections and minimizes virus- and immune-induced injury is essential for developing strategies to contain virus dissemination and disease. While early studies suggested that VEEV enters the CNS via anterograde transport along peripheral nerves after cutaneous inoculation (17), recent findings, however, emphasize that VEEV may cross the BBB via unknown mechanisms (13, 18).

In this study, we show that peripherally inoculated virulent strains of VEEV and WEEV enter the CNS from the bloodstream as free virions through an intact BBB. While VEEV and WEEV interact, enter, and traverse brain endothelium *in vivo*, virus replication within brain microvascular endothelial cells (BMECs) and pericytes is inhibited by type I interferon (IFN) signaling. Consistent with this, reporter and nonreplicative strains of VEEV and WEEV were observed to first replicate within astrocytes and neurons, respectively, suggesting that alphaviruses cross the BBB without replication in BMECs or pericytes. Using an *in vitro* transcytosis assay, alphaviruses were found to utilize caveolin-mediated transcytosis (Cav-MT), which is directly regulated by small Rho GTPases and, notably, IFN. Transmission and immunoelectron microscopy revealed *in vivo* virus encounter and entry at the BBB, with detection of VEEV within caveolin-1-expressing BMECs. Importantly, deficiency in *Cav-1* significantly delayed alphavirus neuroinvasion during early infection, highlighting the important role of caveolae in CNS entry. Together, these data suggest that IFNs regulate the CNS entry of encephalitic alphaviruses via direct and indirect mechanisms.

RESULTS

Alphavirus neuroinvasion occurs prior to BBB disruption. To address mechanisms of alphavirus neuroinvasion in susceptible hosts, we infected mice with enzootic VEEV ZPC-738 (VEEV) and epizootic WEEV McMillan (WEEV) strains of alphaviruses (19,

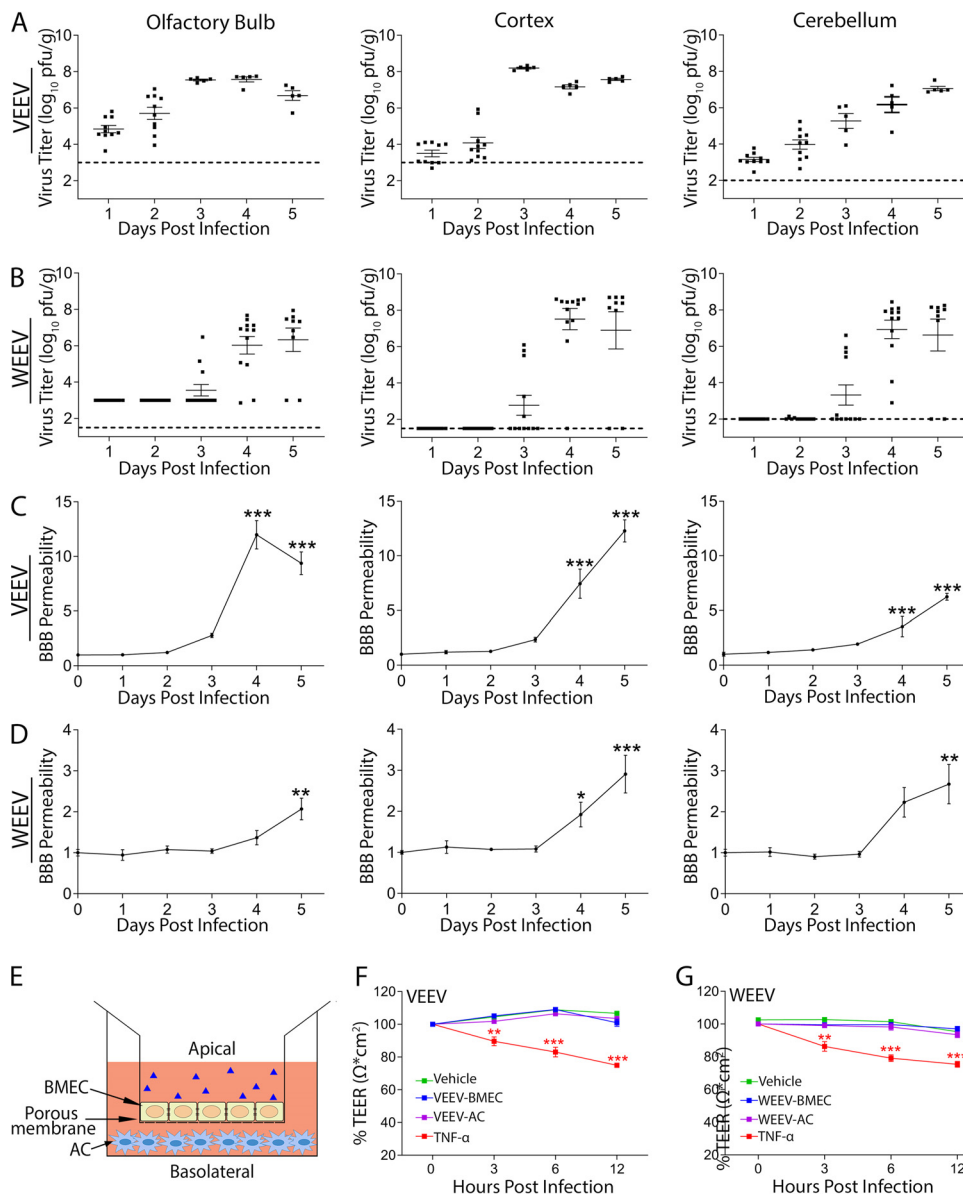


FIG 1 Alphavirus infection of the CNS occurs prior to BBB disruption. (A and B) Viral burdens in brain tissues of C57BL/6 mice following f.p. infection with either VEEV (10 PFU) or WEEV (1,000 PFU), determined by plaque assay. Dashed lines indicate the limit of detection of the assay. Viral burdens were measured at 1 dpi (VEEV) and 3 dpi (WEEV). (C and D) BBB permeability was determined at indicated dpi by measuring sodium fluorescein in CNS tissues following intraperitoneal administration. Data are presented as mean viral titer or fluorescence \pm standard error of the mean (SEM) for $n = 5$ to 10 mice/group. *, $P < 0.05$; **, $P < 0.01$; ***, $P < 0.001$, via 1-way analysis of variance (ANOVA). (E) A schematic figure of an *in vitro* BBB model. AC, astrocyte. (F and G) Neither exposure of BMECs nor exposure of ACs to VEEV and WEEV had any effects on barrier integrity. Addition of TNF- α (100 ng/ml) significantly reduced TEER over time. TEER values for each replicate are presented as normalized values, relative to their respective TEER obtained at 0 h; absolute TEER values were in the 100-to-110 range ($\Omega \cdot \text{cm}^2$). The experiment was performed twice, each with 6 replicates. Error bars indicate mean \pm SEM. Statistically significant differences were determined via 2-way ANOVA followed by Dunnett's multiple-comparison test.

20). Wild-type mice infected with VEEV and WEEV via footpad (f.p.) inoculation exhibited detectable virus replication simultaneously in both fore- and hindbrain regions at 1 and 3 days postinfection (dpi), respectively (Fig. 1A and B). Similar results were observed in the brainstem and spinal cord (see Fig. S1A to D in the supplemental material). Consistent with prior studies, the olfactory bulb exhibited higher VEEV titers at early time points (17). Viral titers plateaued at 10^7 to 10^8 PFU/g of tissue by 3 to 4 dpi (VEEV) and 4 to 5 dpi (WEEV). Significant alterations in BBB permeability occurred at

plateau viral loads in both VEEV- and WEEV infected animals (Fig. 1C and D). Peak BBB permeability in the brainstem and spinal cord also occurred at time points coinciding with peak viral loads (Fig. S1C and D). We also examined direct effects of virus on BBB integrity using an *in vitro* BBB model, in which primary murine BMECs are cultured on transwell inserts over primary murine astrocytes in the bottom chamber (Fig. 1E). In this model, barrier integrity is assessed by measuring transendothelial electrical resistance (TEER) between the transwell chambers. While control cultures treated with tumor necrosis factor alpha (TNF- α) (100 ng/ml) displayed decreased TEER at all time points, addition of virus to either BMECs or astrocytes had no effect on TEER (Fig. 1F and G). To determine whether alphavirus infection of the CNS is associated with alterations in tight junctions (TJ), we used an intranasal (i.n.) infection model in which VEEV is administered into the nasal cavity of mice. In this model, VEEV utilizes retrograde transport along olfactory sensory neurons and hematogenous routes of neuroinvasion with similar kinetics of viral burdens and BBB permeability throughout the CNS as observed after f.p. inoculation (Fig. S2A and B). Claudin-5 is the most predominant claudin found in BBB TJ, with genetic deletion leading to uncontrolled BBB leakage and perinatal death (21). Because claudin delocalization from TJ is sufficient to elicit TJ permeability change independently of its total cellular abundance (22), we quantified the claudin-5 protein abundance levels in BBB TJ from animals infected with VEEV via direct visualization of claudin-5 protein within the TJ via immunogold labeling in ultrathin electron microscopy (EM) sections. Consistent with the BBB permeability data, established VEEV infection (6 dpi) significantly reduced the claudin-5 protein abundance level within the endothelial TJ, while acute infection (from 12 h to 4 dpi) was without significant effect (Fig. S2C and D). Together, our observations from *in vivo* and *in vitro* experiments suggest that alphavirus neuroinvasion occurs in the presence of an intact BBB.

Hematogenous route of neuroinvasion is not exclusive to the CVOs. Viral neuroinvasion across an intact BBB could occur via virus replication within cellular constituents of the NVU. To assess viral permissivity of NVU cells, we examined *in vitro* alphavirus infection of isolated murine cells and performed multistep growth curve analyses after infection with either VEEV (Fig. S3A to C) or WEEV (Fig. S3E to G). While all cell types were permissive to both viruses, slopes of the curves differed; thus, virus replication plateaued as early as 6 to 12 h postinfection (hpi) in astrocytes, while pericytes and BMECs required 12 to 24 hpi and 24 to 48 hpi, respectively, to reach plateau levels. To validate these findings in murine BMECs, the experiment was performed using the human brain endothelial cell line hCMEC/D3, which displayed similar results (Fig. S3D and H). These data suggest that differential restriction of alphavirus replication may occur at the NVU. To examine this *in vivo* during early viral neuroinvasion, we infected mice with 10^6 PFU of either VEEV-enhanced green fluorescent protein (eGFP) or WEEV-eGFP via intravenous (i.v.) injection, followed by immunohistochemical (IHC) detection of GFP within brain tissues. Given the 2-day delay in detection of WEEV compared with VEEV within the CNS (Fig. 1), CNS tissues of VEEV-infected mice were examined at 16 hpi, while WEEV-infected mice were examined at 48 hpi. Analyses of brains revealed multiple foci of viral replication throughout the brain for both viruses, suggesting hematogenous routes of CNS entry. While some of the entry sites overlapped with areas consistent with circumventricular organs (CVOs) (Fig. 2A and B, arrows) (13), others were located within cortical and cerebellar areas that are distant from these structures (Fig. 2A and B, arrowheads). In VEEV-infected mice, GFP expression was detected in both NeuN⁺ neurons and S100- β ⁺ astrocytes (Fig. 2C). In contrast, WEEV-infected animals exhibited GFP expression exclusively within neurons (Fig. 2D). Notably, neither reporter strain led to early viral replication within BMECs or pericytes (Fig. 2C and D), which is consistent with their diminished permissivity *in vitro* compared with astrocytes. Together, these data suggest that cells of the NVU are differentially susceptible to alphavirus infection *in vivo* and that, upon viremia, alpha-

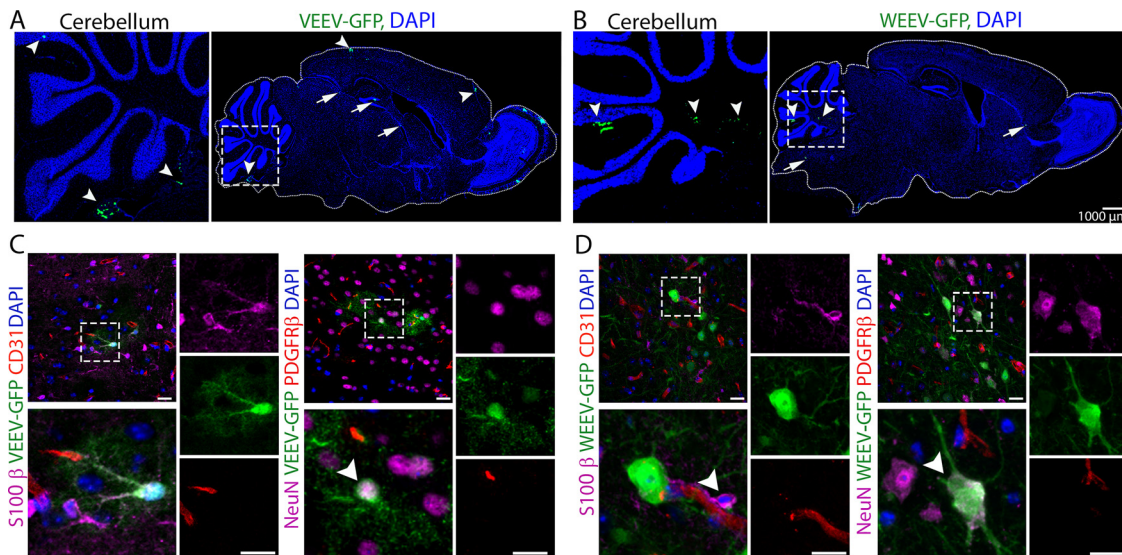


FIG 2 Hematogenous route of alphavirus neuroinvasion is not exclusive to CVOs. (A and B) Low magnification of a sagittal section of VEEV-eGFP (A)- and WEEV-eGFP (B)-infected mouse brain showing multiple entry sites for CNS entry. Arrows indicate entry sites consistent with CVOs. Arrowheads indicate entry sites distant from CVOs. (C and D) Brain tissues from VEEV-eGFP (C)- and WEEV-eGFP (D)-infected mice were stained for markers of astrocytes (S100- β , magenta, arrowhead), BMECs (CD31, red), pericytes (PDGFR- β , red), and neurons (NeuN, magenta, arrowhead). Insets are enlarged in lower left of each panel. Single channels relate to the enlarged insets. Nuclei were counterstained with DAPI (blue). Magnification, $\times 40$; bars, $20 \mu\text{m}$.

viruses invade the CNS from the bloodstream through multiple entry sites that are not exclusive to CVOs.

IFNAR signaling differentially restricts alphavirus infection at the BBB. Given our results demonstrating differential *in vivo* replication of alphaviruses within cells of the NVU, we hypothesized that robust postentry restriction may be imposed by innate immune responses within BMECs and pericytes. To address this, wild-type (WT) and *Ifnar*^{-/-} mice were infected with VEEV-eGFP (100 PFU) via f.p. inoculation, and brain tissues were examined at 1 dpi for GFP expression. Notably, *Ifnar*^{-/-} mice succumb to VEEV-eGFP by ~ 30 h postinfection (Fig. S4A), while WT animals have undetectable brain infection using IHC at this time point (Fig. S4D). Thus, to allow comparisons at similar viral burdens (Fig. S4C), we also evaluated brain tissues of WT mice at 3 dpi. VEEV infection was limited to S100- β ⁺ astrocytes and NeuN⁺ neurons in WT animals (Fig. 3A and Fig. S5A), whereas similar infection in *Ifnar*^{-/-} animals led to GFP expression within BMECs and pericytes in both the cortex (Fig. 3B) and cerebellum (Fig. S5B). Next, we assessed cellular tropism in the context of WEEV-eGFP (1,000 PFU) infection. Although mortality was significantly increased in WEEV-eGFP-infected *Ifnar*^{-/-} mice compared with similarly infected WT animals, *Ifnar*^{-/-} mice survive WEEV infection up to 5 to 6 dpi (Fig. S4B), and viral infection was undetectable in brain tissues of either WT or *Ifnar*^{-/-} mice at 1 dpi (Fig. S4E). Thus, brain tissues were examined at 3 dpi for both genotypes. Similarly to our observations with VEEV, WT mice infected with WEEV exhibited no GFP expression in BMECs or pericytes, with infection detected only in neurons (Fig. 3C and Fig. S5C). However, *Ifnar*^{-/-} mice additionally exhibited GFP expression within cortical (Fig. 3D) and cerebellar (Fig. S5D) astrocytes.

As the observed changes in cellular tropism could be due to a higher titer of viremia in *Ifnar*^{-/-} than in WT mice, *Ifnar*^{-/-} mice were infected with 10^6 PFU/ml of a nonreplicative (NR) replicon derived from VEEV-eGFP (23), a physiologically relevant dose that is equivalent to the level of viremia observed in WT mice after f.p. inoculation (Fig. S5F). Following cellular entry, NR-VEEV-eGFP undergoes RNA replication and produces reporter gene products, but no progeny virus, due to lack of structural genes (23). Similarly to our results with WT VEEV-eGFP, WT animals infected with NR-VEEV-eGFP had no infection of BMECs or pericytes (Fig. 3E), whereas *Ifnar*^{-/-} mice exhibited

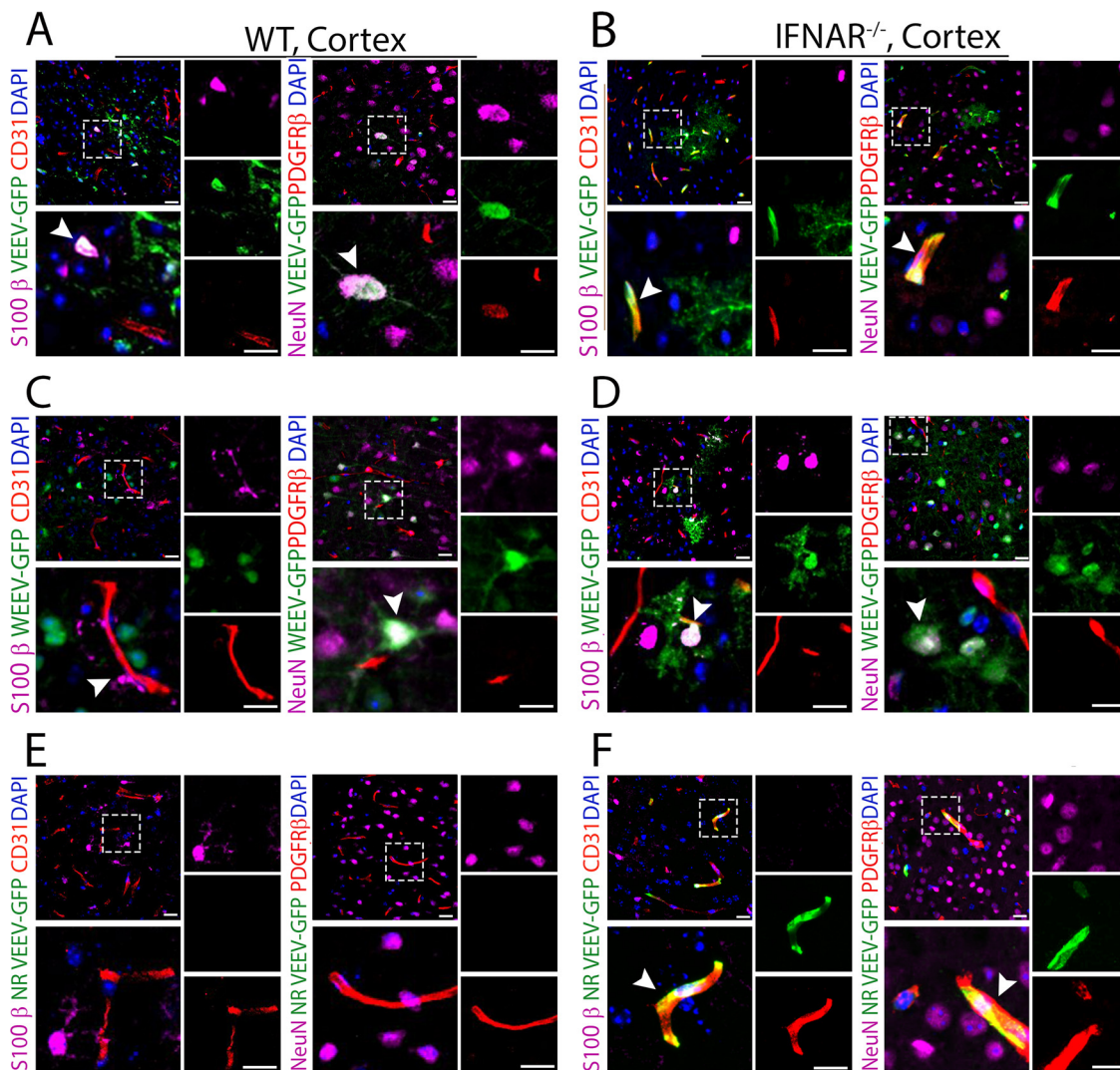


FIG 3 Type I IFNs differentially restrict alphavirus replication within the NVU. (A to D) IHC staining of cortical brain regions of WT (A and C) and *Ifnar*^{-/-} (B and D) mice following f.p. infection with either VEEV-eGFP (A and B) or WEEV-eGFP (C and D). Cell markers were as follows: S100- β for astrocytes, CD31 for BMECs, PDGFR- β for pericytes, and NeuN for neurons. Nuclei were counterstained with DAPI (blue). (E and F) IHC staining of cortical brain regions of WT (E) and *Ifnar*^{-/-} (F) mice following i.v. infection with NR-VEEV-eGFP. Magnification, $\times 40$; bars, 20 μ m.

extensive infection of these cell types in multiple brain regions, including the cortex (Fig. 3F) and cerebellum (Fig. S5E). These findings support the notion that alphavirus infection is differentially restricted at the NVU by IFNAR signaling, which prevents CNS entry by blocking active virus replication within BMECs.

Ultrastructural analysis reveals alphavirus interaction and entry at the BBB. To further characterize virus-cell interactions at the BBB *in vivo*, we performed transmission electron microscopy (TEM) of CNS tissues derived from VEEV-infected WT and *Ifnar*^{-/-} mice. TEM analysis of *Ifnar*^{-/-} mice, which develop high level of viremia (Fig. S5F), revealed 70-nm spherical structures with electron-dense cores, consistent with virions (24), attached to the luminal surface of cortical microvessels (Fig. 4A). Additionally, immunogold labeling using antibodies (Abs) against the VEEV E2 glycoproteins detected viral particles inside cortical BMECs of WT mice (Fig. 4B). Since WT BMECs do not support VEEV replication *in vivo* (Fig. 3A), detection of E2 glycoproteins likely represents an intact virion rather than intracellular protein expression. Based on these observations, we hypothesized that VEEV may cross the BBB as free particles. To examine this, mice were infected with NR-VEEV-eGFP via i.v. injection. At 1 dpi, we detected infection

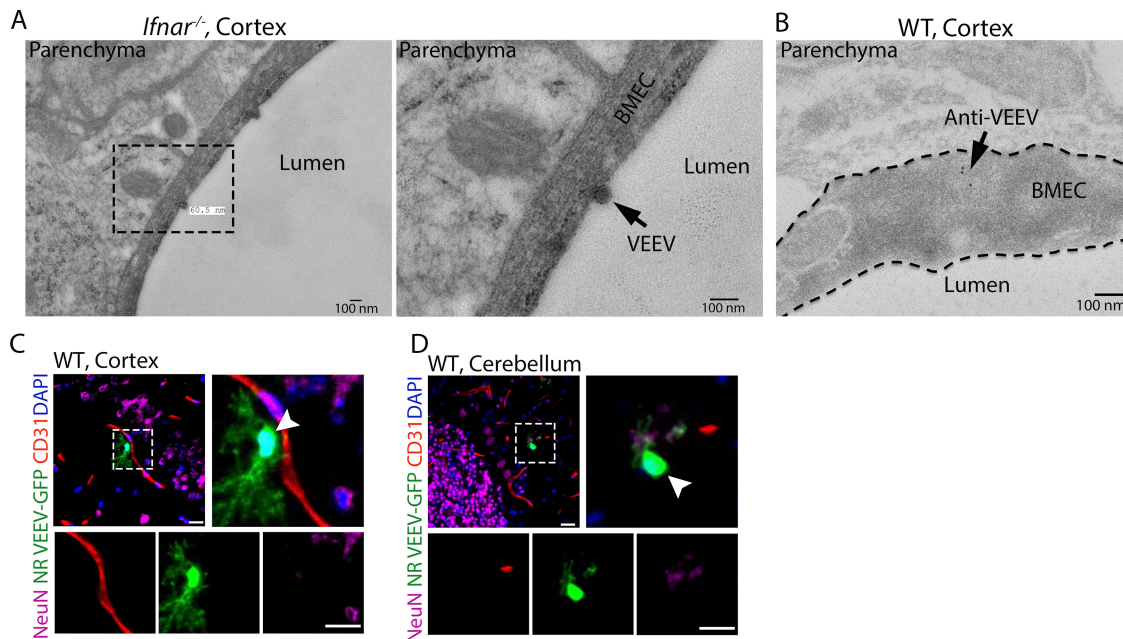


FIG 4 Detection of alphavirus interaction and entry at the BBB. (A) TEM analysis of brain tissues from VEEV-infected mice at 1 dpi identified virus-like particles attached to the luminal surface of microvessels. (B) Viral E2 glycoproteins were detected within cortical BMECs of VEEV-eGFP-infected mice (3 dpi) by immuno-EM using 8-nm immunogold particles. Bars, 100 nm. (C and D) Immunostaining of brain tissues collected from NR-VEEV-eGFP-infected WT mice at 1 day following i.v. infection. Cell markers were as follows: CD31 for BMECs and NeuN for neurons. Nuclei were counterstained with DAPI (blue). Arrowheads indicate infected astrocyte-like cells. Magnification, $\times 40$; bars, 20 μm .

of astrocyte-like cells in multiple brain regions, including cortex and cerebellum (Fig. 4C and D), suggesting that VEEV can cross the BBB as free virions, likely via a transcytosis mechanism.

Alphavirus crosses brain endothelial cells via caveola-mediated transcytosis.

Based on our TEM data (Fig. 4A and B), we hypothesized that alphaviruses may exploit BMEC endocytic machinery for entry across the BBB. In contrast to peripheral tissues, the rate of transcytosis and numbers of endocytic vesicles are relatively low in BMECs (5). However, exposure of BMECs to VEEV or WEEV (multiplicity of infection [MOI] of 10) resulted in enhanced caveola formation at the cell surface (Fig. 5A to D). We next quantified the number of caveola-like structures in BMECs of VEEV-infected mice. Similar to our *in vitro* data, we observed increased vesiculation in cytoplasm and at the luminal surface of BMECs in infected animals (Fig. 5E to G). In addition, virus infection induced membrane ruffling in BMECs of infected mice (Fig. 5H). These observations suggest a possible mechanism for viral transcytosis. To address this, we utilized a transcytosis assay in which virus is added to the top chambers of transwell inserts for 60 min, followed by removal of inserts and assessment of infectious virions in the bottom chamber (Fig. 6A). As the replication time of VEEV in BMECs is approximately 3 to 6 h (Fig. S6A), virus detected in the bottom chamber is unlikely due to replication, which was confirmed by assessment of GFP expression in bottom chamber astrocytes after transcytosis of NR-VEEV-eGFP virus (Fig. 6B). TEM evaluation of virus transcytosis across BMECs additionally identified virion-like structures within endosomes, characteristic of caveolae (25). Virion-containing endosomes were detected at various stages of transcytosis, i.e., early endosomes, multivesicular bodies, and exocytic vesicles within infected BMECs (Fig. 6C to E). Together, these data suggest that VEEV has the ability to cross the endothelial cell barrier via a transcytosis mechanism.

Transcytosis may utilize various pathways, including macropinocytosis and clathrin- or caveola-mediated endocytosis (CME or Cav-ME, respectively) (6, 26), which may be interrogated via use of inhibitors including amiloride hydrochloride (macropinocytosis); filipin, nystatin, and cholesterol oxidase (Cav-ME); and chlorpromazine (CME). Com-

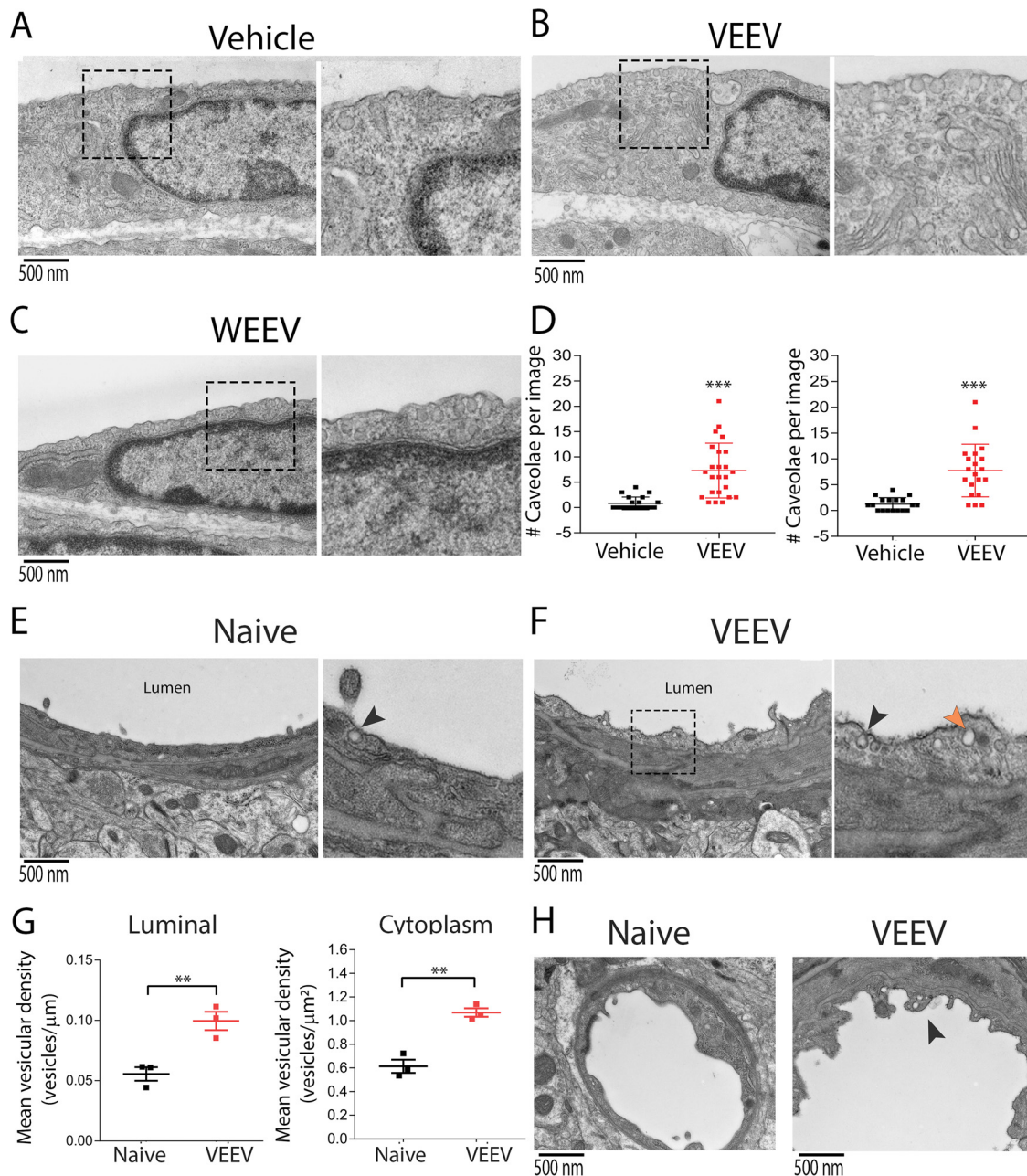


FIG 5 Alphavirus infection enhances caveola formation in brain endothelial cells. (A to C) Exposure of BMECs to either VEEV or WEEV at an MOI of 10 enhanced caveola formation at the cell surface compared to vehicle. (D) Quantitation of cell surface-associated caveolae in BMECs after virus exposure. Statistical differences were analyzed by 1-way ANOVA followed by Dunnett's multiple-comparison test. ***, $P < 0.001$. (E and F) TEM analysis of brain tissues collected from naive and VEEV-infected mice at 3 dpi. Black arrowheads indicate luminal caveola-like structures. Orange arrowhead indicates intracellular vesicle. (G) Quantitation of caveola-like structures at the cell surface and inside the cytoplasm of brain endothelial cells of naive versus infected animals. Three tissue blocks were harvested from the cortical brain region of each mouse ($n = 3$ in each group), and 30 images were obtained per block. After manual counting, the mean vesicular density per length or volume of cytoplasm was calculated using ImageJ (NIH). Statistical differences were analyzed using the t test. (H) TEM analysis demonstrating membrane ruffling (arrowhead) in BMECs of infected mice relative to control animals.

pared with untreated BMECs or hCMEC/D3, the percentage of transcytosis for both VEEV and WEEV was significantly reduced in the presence of inhibitors of Cav-ME but not CME or macropinocytosis (Fig. 6F to I). Notably, none of the inhibitors affected viral infectivity or barrier integrity (Fig. S6B to E). In accordance with the key role of caveolin-1 in caveola formation, *Cav-1*^{-/-} BMECs displayed diminished virus transcy-

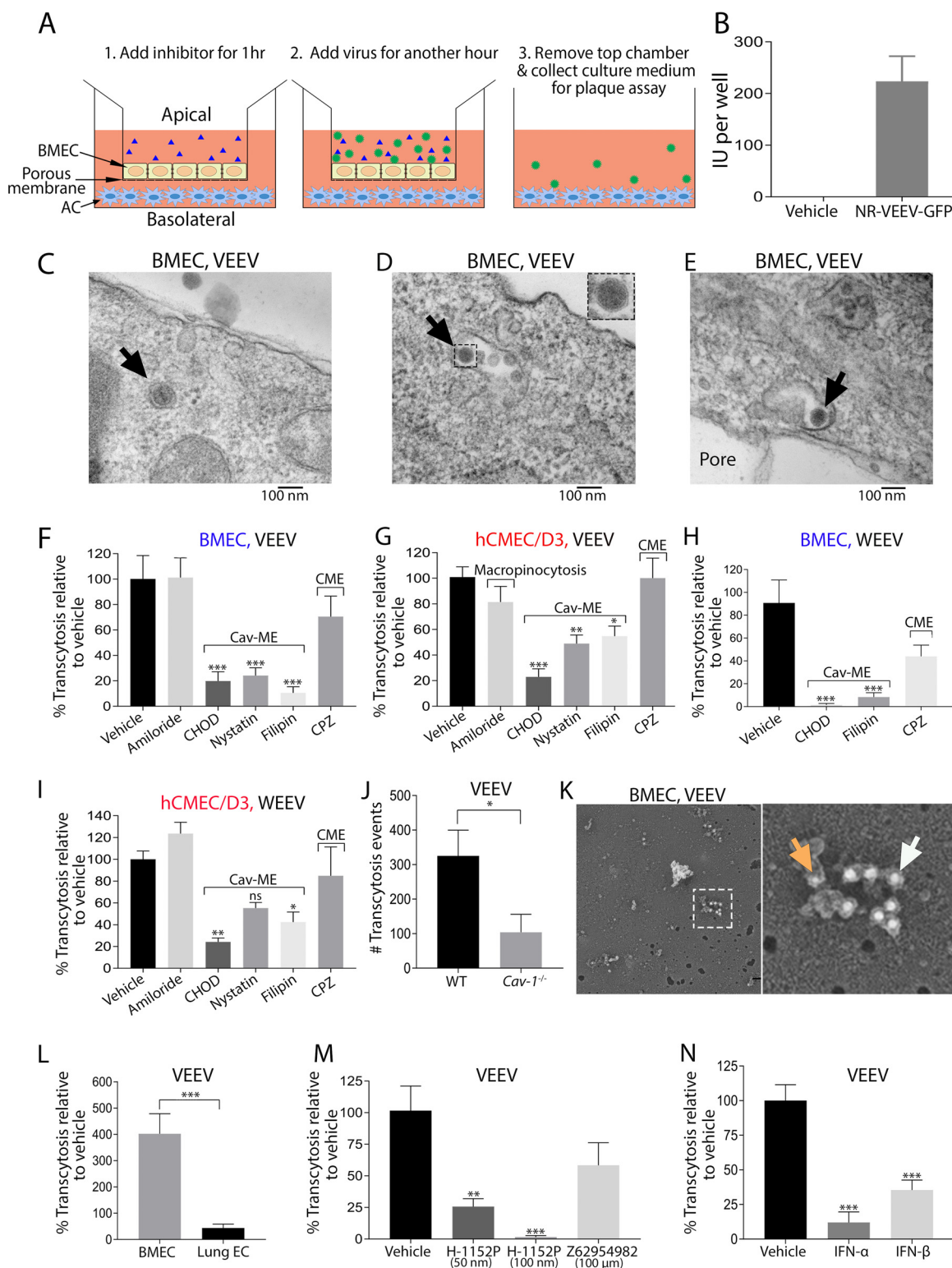


FIG 6 Alphavirus crosses BMECs via caveola-mediated transcytosis. (A) A schematic figure demonstrating different steps of a transcytosis assay. (B) Addition of a nonreplicative strain of VEEV-eGFP to hCMEC/D3 on the top chamber resulted in GFP signals in human astrocytes in the bottom chamber. (C to E) TEM analysis identified virus-like particles (depicted by arrows) within early endosomes (C), multivesicular bodies (D) and exocytotic endosomes (E) in BMECs after exposure to VEEV for 30 min. (F to I) VEEV and WEEV traverse monolayers of BMECs (F and H) and hCMEC/D3 (G and I) via caveola-mediated transcytosis. Data are presented as mean percentage of transcytosis relative to untreated cells. Experiments were repeated 2 to 3 times each with 4 to 6 technical replicates. Error bars indicate standard errors of the means (SEM). Concentrations of inhibitors are shown in parentheses: amiloride hydrochloride hydrate (50 μM), cholesterol oxidase (CHOD; 2 U/ml), filipin (1 μg/ml), nystatin (12 μg/ml), and chlorpromazine (CPZ; 10 μg/ml). (J) Quantitation of VEEV transcytosis across WT and Cav-1^{-/-}. (Continued on next page)

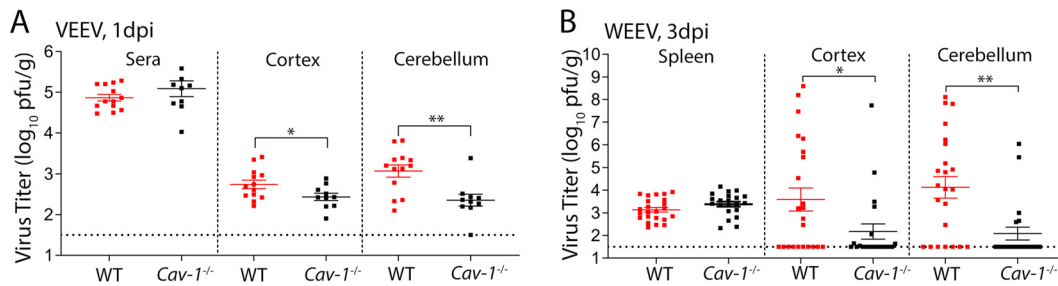


FIG 7 *Cav-1*^{-/-} mice displayed reduced viral titers in the brain compared to WT animals. (A and B) Viral burdens in peripheral and brain tissues of WT versus *Cav-1* knockout mice after f.p. infection with VEEV (10 PFU) and WEEV (1,000 PFU), determined by plaque assay. Error bars indicate standard errors of the means (SEM). Shown are the combined data from 4 independent experiments each with 4 to 6 animals. Results were analyzed by unpaired *t* test: *, *P* < 0.05; **, *P* < 0.01.

toxicity compared to WT cells (Fig. 6J). These results were further verified using freeze fracture electron microscopy, wherein we identified VEEV particles (8-nm gold particle; orange arrow) colocalized with Cav-1⁺ (16-nm gold particles, white arrow) (Fig. 6K). In addition, lung endothelial cells exhibited significantly reduced virus transcytosis compared to BMECs (Fig. 6L), suggesting specificity of alphavirus transcytosis for BMECs.

Caveola formation is enhanced by the small Rho GTPase RhoA, which is inhibited by Rac1 activity (27, 28). Thus, we sought to evaluate virus transcytosis across BMECs in the absence and presence of either Rho kinase inhibitor (H-1152, 50 nM and 100 nM) or Rac-1 inhibitor (Z62954982, 100 μM) (11, 29–32). While H-1152 significantly reduced VEEV transcytosis across BMECs, Z62954982 had no significant effect on virus transmigration (Fig. 6M). However, treatment with IFN-α or IFN-β, which has been shown to promote BBB tight junction integrity via activation of Rac-1 (11), significantly reduced VEEV transcytosis, suggesting direct effects of IFNAR signaling on Cav-MT (Fig. 6N). Together, these results indicate that VEEV and WEEV exploit Cav-1-MT to cross an intact BBB and that this may be regulated by IFN.

Caveolin-1 contributes to alphavirus neuroinvasion *in vivo*. To validate the role of caveolin-1 in early alphavirus neuroinvasion *in vivo*, we infected WT and *Cav-1*^{-/-} mice with either VEEV (10 PFU) or WEEV (1000 PFU) via f.p. infection and examined peripheral and CNS viral burdens at 1 and 3 dpi. As WEEV could not be detected in sera, we examined splenic tissues. Both VEEV- and WEEV-infected *Cav-1*^{-/-} mice exhibited significantly reduced viral titers in the cortex and cerebellum at 1 dpi and 3 dpi, respectively, compared to similarly infected WT animals, whereas viral burdens in the serum and spleen were indistinguishable between the two genotypes (Fig. 7A and B). Importantly, no differences in CNS viral loads were detected in intracranial alphavirus-infected WT compared with *Cav-1*^{-/-} mice (Fig. S7A and B), indicating no effect of Cav-1 deficiency on viral replication within the CNS. These results indicate that while Cav-MT is not the sole route of CNS entry by encephalitic alphaviruses, it significantly contributes to viral seeding into the CNS following peripheral infection.

DISCUSSION

Using *in vitro* and *in vivo* approaches, we examined early events during alphavirus neuroinvasion. We found that VEEV and WEEV can enter the CNS via hematogenous dissemination across an intact BBB, without viral replication within BMECs or pericytes, leading to productive infection of CNS-resident cells. Differential restriction of viral infection within cellular constituents of the NVU is mediated by IFNAR signaling, with

FIG 6 Legend (Continued)

Cav-1^{-/-} BMECs. (K) Immunogold labeling of virally infected BMECs revealed VEEV (8-nm immunogold particles; orange arrow) in colocalization with caveolin-1 (16-nm immunogold particles; white arrow). (L) VEEV transcytosis percentages were compared between brain and lung ECs. (M and N) VEEV transcytosis across BMECs in the absence and presence of Rho kinase GTPase (H-1152P) and Rac-1 (Z62954982), as well as type I IFNs (100 pg/ml). Results from transcytosis assays were analyzed by 1-way ANOVA (F to I, M, and N) and *t* test (J and L). *, *P* < 0.05; **, *P* < 0.01; ***, *P* < 0.001.

replication in BMECs and pericytes (VEEV) and astrocytes (WEEV) observed only in *Ifnar*^{-/-} mice. VEEV and WEEV entry across the BBB occurs via Cav-MT, which is impeded by Rho kinase inhibitor and IFN, the latter likely via activation of Rac1 (11, 12). Immuno-EM demonstrated alphavirus interaction, internalization, and Cav-1 association within BMECs both *in vitro* and *in vivo*. Consistent with this, Cav-1 deficiency reduced alphavirus transcytosis *in vitro* and led to reduced titers of VEEV or WEEV in the CNS during early infection *in vivo*. Taken together, these data suggest that innate immune signaling regulates alphavirus neuroinvasion and replication at the NVU.

The CNS entry of alphaviruses following peripheral infection has been shown to occur via multiple routes. Early studies in mice indicated that VEEV may reach the brain via retrograde transport along peripheral nerves (17), whereas, more recently, VEEV and other encephalitic alphaviruses have been shown to enter the CNS directly from the bloodstream (13, 14, 33). In our study, peripheral infection of mice with virulent strains of VEEV and WEEV resulted in detectable viral loads at time points that precede BBB disruption (Fig. 1), and neither VEEV nor WEEV induced alterations in TEER across an *in vitro* BBB. These results indicate that alphaviruses cross the BBB shortly after infection without affecting barrier integrity. Hematogenous routes of neuroinvasion may include viral passage through the CVOs, which lack specializations that comprise the BBB (13). Our study demonstrated that shortly after i.v. infection (16 h), foci of alphavirus infection are observed simultaneously in cortical and cerebellar locations distant from the CVOs, suggesting that CNS entry is not exclusive to these structures. Notably, BBB breakdown occurs at later time points, when viral loads have peaked. This is likely due to induction of matrix metalloproteinase 9 (MMP-9) within CNS tissues that disrupts the tight junction proteins between brain endothelial cells (18). Additionally, induction of inflammatory immune responses (e.g., TNF and interleukin 6 [IL-6]) and upregulation of cell adhesion molecules (e.g., ICAM-1 and vascular cell adhesion molecule 1 [VCAM-1]) on brain endothelium allows immune cell interaction and infiltration at the BBB, further contributing to barrier disruption (18, 34, 35).

Pathogens, including viruses, may cross the BBB via direct infection of brain endothelium (36, 37). Use of reporter and nonreplicative strains of VEEV and WEEV during *in vivo* infection, however, indicated lack of infection within BMECs (Fig. 3), suggesting that active virus replication in brain endothelium does not contribute to CNS entry. VEEV has a broad tissue tropism and can infect many cell types, including macrophages and dendritic cells (23). Infected leukocytes may act as Trojan horses and introduce viral particles into the CNS upon infiltration. However, leukocyte interaction and extravasation at the BBB require elevated expression of cell adhesion molecules (CAMs) on brain endothelium, which does not occur until 3 dpi (18). Since we detected significant viral loads throughout the CNS by 1 dpi (Fig. 1), it is unlikely that infected leukocytes are the initial source of virus in the CNS. Importantly, our data using NR-VEEV-eGFP did not detect viral infection within CNS-infiltrating leukocytes, suggesting that virus can enter CNS as free virions and independent of leukocyte trafficking. Nonetheless, additional studies are required to precisely define the role of a Trojan horse in alphavirus neuroinvasion.

Our TEM analysis demonstrated virus-like particles attached to the lumen of brain endothelium. Given that viremia arises as early as 8 h after VEEV infection, BMECs are likely among the first cell types exposed to virions. Such exposure may trigger innate immune responses (e.g., type I IFNs), which can influence intercellular communication at the NVU (38). Indeed, in the context of IFNAR deficiency, VEEV and WEEV replicate within BMECs and astrocytes, respectively. The lack of viral replication within these cellular constituents of the NVU in WT animals is likely due to paracrine effects of IFN that induce antiviral proteins, as has been recently reported for arthritogenic alphaviruses (39, 40). VEEV attachment to and internalization within BMECs were further confirmed via immuno-TEM, in which viral E2 glycoproteins were detected within these cells, supporting the notion that alphaviruses may cross the BBB via a transcytosis pathway.

Compared to peripheral tissues, the rate of transcytosis at the BBB is unusually low.

However, this rate may be augmented by increased Src kinase activity, which is mediated by a group of pathological and nonpathological stimuli, including inflammatory mediators and immune cell interactions with brain endothelium (41). Viruses may also increase vesicular trafficking, as has been observed in peripherally derived endothelial cells exposed to dengue virus (42). In our study, we utilized both *in vitro* assays and *in vivo* viral infection models and observed that both VEEV and WEEV induce formation of caveolae in BMECs. *In vivo*, VEEV-infected mice exhibited increased vesiculation and membrane ruffling within brain endothelial cells (Fig. 5). *In vitro* studies have shown that alphaviruses may induce dramatic structural changes in the actin cytoskeleton, leading to the formation of filopodium-like extensions in infected cells (43). Notably, expression of the viral nonstructural protein 1 (nsP1) alone is sufficient to trigger formation of short extensions, which is dependent on its palmitoylation activity (44). Consistent with this, ablation of nsP1 palmitoylation sites abolishes the ability of Semliki Forest virus (SFV) to infect the brain in murine models (45). Elucidating molecular mechanisms underlying alphavirus-induced vesiculation in BMECs may reveal therapeutic targets against viral neuroinvasion and provide insights for BBB maintenance in the context of other neurological disorders induced by increased transcytosis in brain endothelium (46–48).

Transcytosis of macromolecules across brain endothelium predominantly occurs via mechanisms that utilize caveolae. During infectious diseases, interaction with caveolae allows pathogens to escape lysosomal degradation and cross endothelial cell barriers (49, 50). While different families of viruses have been shown to cross epithelial and endothelial cell barriers utilizing Cav-MT *in vitro* (51–53), *in vivo* findings to support these data have been difficult to obtain, especially within the brain, where these events are rare. Our study utilized multiple approaches to demonstrate that neurotropic alphaviruses enter but do not replicate within brain endothelium and that Cav-MT contributes to *in vivo* viral infection of the CNS. As peripherally infected *Cav-1*^{-/-} mice exhibit a delay in achievement of peak brain titers of VEEV and WEEV compared to WT animals, entry of virus in the absence of caveolae may rely on slower mechanisms of viral entry, such as retrograde transport along axons (17). Additionally, recent studies have shown that encephalitic alphaviruses can gain access to the CNS by viral passage through the CVOs, which lack the normal BBB (13). Further, ablation of caveolin-1 results in upregulation of caveolin-independent pathways (54), which might explain how viral loads within CNS tissues derived from *Cav-1*^{-/-} mice quickly attain the levels observed in WT animals.

The signaling cascade underlying transcytosis was further elaborated using *in vitro* assays, wherein deficiency in caveolin-1 or depletion of membrane cholesterol significantly reduced VEEV and WEEV transcytosis across the BMEC monolayer. Notably, virus transcytosis across brain endothelial cells was blocked by Rho kinase inhibitor (Fig. 6). The Rho family of GTPases, including RhoA, Rac-1, and Cdc42, are known to play a role in pathogen uptake and dissemination within the host (55–58). These proteins alternate between an active GTP-bound form and an inactive GDP-bound form which triggers rearrangements in the actin cytoskeleton and cellular uptake of pathogens (59). Studies in flavivirus encephalitis have shown that IFN- β acts in synergy with the Tyro3/Axl/Mer (TAM) receptor Merck to activate Rac-1, which enhances BBB tight junction integrity, thereby preventing paracellular entry of virus (11, 12). In the current study, we discovered that type I IFN also prevents alphavirus transcytosis across BMECs. Thus, although the VEEV nsP2 and capsid protein inhibit IFN signaling via host shutoff (60), the lack of viral replication within BMECs may allow IFN signaling to limit viral entry likely via modulation of Rho GTPases (11).

In summary, mechanisms of encephalitic alphavirus neuroinvasion from the blood are complex and may depend on individual viral tropism for olfactory sensory neurons and cellular constituents of the NVU, which provide avenues of entry that cross the BBB, respectively (23, 61). Neuroinvasion may also depend on innate immune mechanisms that exert virus- and cell-specific effects on replication (60). Ablation of the olfactory route reduces but does not eliminate CNS entry of VEEV (17), suggesting that each route of entry provides a relative contribution to alphavirus neuroinvasion. Further studies are needed to address how each process individually contributes to viral entry

and whether viral spread within the CNS relies on these pathways or on innate immune mechanisms that regulate intracellular viral trafficking and replication within permissive cells. Our data highlighted the critical role of Cav-MT in alphavirus neuroinvasion. Delineating molecular mechanisms involved in this process may reveal novel targets for potential therapeutic interventions against CNS infection.

MATERIALS AND METHODS

Cells. Baby hamster kidney (BHK-21) and African green monkey kidney (Vero) cells were maintained in Dulbecco's modified Eagle's medium (DMEM) supplemented with 10% fetal bovine serum (FBS) and 100 μ g/ml of penicillin and streptomycin. Primary murine brain microvascular endothelial cells (BMECs), pericytes, and astrocytes were isolated from cortical brain of C57BL/6J mice and maintained in culture as described previously (11, 62). The immortalized human cerebral microvascular endothelial cell line hCMEC/D3 (63) was purchased from Millipore Sigma and maintained in endothelial cell growth basal medium 2 (EBM2; Lonza). Primary human astrocytes and murine lung endothelial cells were purchased from ScienCell Research Laboratories and Cell Biologics, respectively. Cells were maintained in the culture medium recommended by each company.

Antibodies and reagents. Rabbit polyclonal anti-S100- β (ab41548), rabbit monoclonal anticalbindin (ab108404), and rabbit polyclonal anti-red fluorescent protein (anti-RFP) (ab62341) antibodies (Abs) were purchased from Abcam Biotechnology. Purified rat anti-mouse CD31 (550274, clone MEC 13.3) and guinea pig anti-NeuN (ABN90P) polyclonal Abs were purchased from BD Biosciences and Millipore-Sigma, respectively. Goat anti-platelet-derived growth factor receptor beta (anti-PDGFR- β) (AF1042) Ab was purchased from R&D Systems. The anti-VEEV E2 monoclonal antibody was a kind gift from Michael Diamond (Washington University, St. Louis, MO). Amiloride hydrochloride hydrate, filipin, cholesterol oxidase, nystatin, chlorpromazine hydrochloride, Z62954982, and fluorescein sodium salt were purchased from Sigma-Aldrich. (S)-Glycyl-H-1152 (hydrochloride) was purchased from the Cayman Chemical Company. Mouse IFN- α and - β were obtained from PBL Assay Science.

Virus propagation, purification, and titration. All viruses used in this study, including the non-replicative "replicon" strain of VEEV (NR-VEEV-eGFP), replication-competent VEEV, McMillan strain (WEEV), and GFP reporter viruses (64), were generously provided by William Klimstra (University of Pittsburgh, Pittsburgh, PA). The parental VEEV and WEEV cDNAs were gifts to Klimstra from Scott Weaver, University of Texas Medical Branch at Galveston, and Kenneth Olson, Colorado State University, respectively. The McMillan cDNA was modified by placing the entire virus coding region in a pBR322-based plasmid under the control of a T7 bacteriophage promoter. Stocks of VEEV and WEEV viruses were generated as described previously (34). Briefly, BHK-21 cells were infected at a multiplicity of infection (MOI) of 0.1. Culture medium was replaced with fresh medium 4 h later. Virus-containing supernatants were collected on the next day (~30 h postinfection), cleared from cell debris by low-speed centrifugation, and filtered through 0.22- μ m filters. Virus particles were then concentrated by ultracentrifugation at 100,000 \times *g* for 2 h at 4°C through a cushion of 30% (wt/wt) sucrose in phosphate-buffered saline (PBS). The virus pellet was resuspended in PBS and stored in single-use aliquots at -80°C. Titrations of VEEV and WEEV were performed in BHK-21 and Vero cells, respectively.

Multistep growth curves. Primary murine BMECs, astrocytes, and pericytes were seeded in 24-well plates for 3 to 4 days until they reached confluence. At this point, cells were exposed to MOIs of 0.01, 0.1, and 1 of VEEV and WEEV. Culture medium was removed 1 h postinfection, and cells were washed 4 times with 1 ml/well of PBS. The last wash was stored at -80°C, and later it was used in a plaque assay to determine residual unbound virus remaining in each well. Culture supernatant was harvested at specified time points, and virus titer was determined using plaque assay in BHK-21 (VEEV) and Vero (WEEV) cells.

Mouse studies. C57BL/6J wild-type and caveolin-1-knockout mice were purchased from the Jackson Laboratory (Bar Harbor, ME). *Ifnar*^{-/-} mice were kindly provided by Michael Diamond (Washington University School of Medicine, St. Louis, MO). Animals were housed under pathogen-free conditions, and the experimental procedures were completed in accordance with the Washington University School of Medicine Animal Safety Committee. Male, 8- to 9-week-old mice were used in all *in vivo* experiments. Mouse infections were performed by administering virus by either subcutaneous (s.c.), intravenous (i.v.), or intracranial (i.c.) injection, while the mice were under light ketamine anesthesia. For subcutaneous infection, mice were injected in the footpad with VEEV (10 PFU) and WEEV (1,000 PFU) in 50 μ l PBS. Intracranial infections were performed by inoculating 10 PFU (VEEV) or 100 PFU (WEEV) of virus in 10 μ l of PBS into the right cerebral hemisphere via a guided 29-gauge needle. Intravenous infections were achieved by administering 2×10^6 PFU of virus in 100 μ l of PBS via retro-orbital injection. Mock-infected animals received the same volume of PBS in each infection method and were considered controls where needed.

Measurement of viral burden in tissues. To monitor the kinetics of virus spread *in vivo*, peripheral organs and CNS tissues were harvested from infected mice at specified time points. Prior to this, mice were perfused transcardially with 30 ml PBS. Tissues were homogenized in 500 μ l PBS using a MagNA Lyser (6,000 rpm for 1 min) instrument, and virus titer in tissue homogenates was determined using plaque assay in either BHK-21 or Vero cells depending on virus. Alternatively, groups of mice were followed for survival assays.

***In vivo* assessment of BBB permeability.** At given days postinfection, mice received 100 μ l of 100-mg/ml fluorescein sodium salt (NaFL) in PBS via intraperitoneal injection. When the salt reached equilibrium (45 min), blood samples were collected, and mice were perfused transcardially with 30 ml PBS prior to collection of CNS tissues. Serum samples and tissue homogenates were treated with 2% trichloroacetic acid overnight at 4°C to precipitate proteins. Supernatants were clarified from cellular

debris by centrifugation (4,000 rpm for 20 min at 4°C) and diluted in equal volumes of borate buffer, pH 11 (Sigma-Aldrich). Concentration of NaFL in supernatants was determined by measuring fluorescence emission at 538 nm using a Synergy H1 microplate reader (BioTek Instruments, Inc.). Measurement values were normalized to tissue weight and to NaFL plasma concentration in each mouse.

***In vitro* BBB model and transcytosis assay.** An *in vitro* BBB model was generated as described elsewhere (34). Briefly, BMECs were seeded on the apical side of fibronectin-coated inserts (BD Falcon; 24-well, 3- μ m pores). Concurrently, primary murine astrocytes were cultured in fibronectin-coated 24-well plates. Two days later, when astrocytes reached confluence, BMEC inserts were moved to an astrocyte-containing plate. Astrocytes release growth factors that promote barrier formation between BMECs. Culture medium was changed every 3 days. On day 7, hydrocortisone (550 nM), CTP-cAMP (250 μ M), and RO 20-1724 (17.5 μ M) compounds were added to the cells in serum-free medium to further promote expression of tight junctions and barrier formation between BMECs. On the following day, barrier integrity was assessed by measuring transendothelial electric resistance (TEER) before cells were used for transcytosis assay. In these assays, BMECs on the top chamber are exposed to different treatments for 1 to 2 h. Virus particles are then added at an MOI of 2 to BMECs on the top chamber for an additional hour. At this point, BMEC inserts are removed and culture medium is collected from the bottom chamber and is used in plaque assay to determine the number of virus particles that have crossed the BMEC monolayer in the presence and absence of different inhibitors. Exposure of BMECs to alphavirus is limited to 1 h to prevent active virus replication and release of viral progenies from the basolateral side.

Immunohistochemistry and confocal microscopy. Brain tissues were collected from infected mice at specified time points as indicated in each figure legend. Prior to tissue collection, mice were deeply anesthetized and perfused transcardially with 30 ml of PBS followed by 30 ml of 4% paraformaldehyde (PFA). Tissues were stored overnight in 4% PFA in PBS at 4°C and then transferred into two exchanges of 30% sucrose for 48 h, before they were embedded in O.C.T. compound (Tissue-Tek). Ten-micrometer cryostat brain sections were treated with proteinase K (5 μ g/ml for 30 min at room temperature [RT]) for antigen retrieval. After a 30-min incubation in blocking buffer, tissue sections were stained with primary antibodies to markers for astrocytes (S100 calcium-binding protein [S100]- β), pericytes (platelet-derived growth factor receptor beta [PDGFR- β]), BMECs (CD31), and neurons (NeuN and calbindin). Sections were then incubated with appropriate secondary antibodies (Alexa Fluor 488 and 555 and DyLight 650, all from Invitrogen) for 15 min in blocking buffer, followed by three washes in PBS. After antibody labeling, cells were counterstained with 4',6-diamidino-2-phenylindole (DAPI) (D1306; Invitrogen). All images were obtained using a confocal microscope (Carl Zeiss) and processed with ImageJ software (NIH).

Transmission and immunogold electron microscopy. For TEM, mice underwent cardiac perfusion with 5 ml of PBS, followed by 20 ml of 1.5% glutaraldehyde and 1% PFA in 0.12 M sodium pyrophosphate buffer, while for immuno-EM studies, perfusion was performed with 5 ml of PBS and 20 ml of 4% paraformaldehyde in 0.12 M sodium pyrophosphate buffer. Brain tissues were then collected and stored in fixative buffer overnight at 4°C and processed as previously described (34). For immuno-EM, ultrathin brain sections (70 nm) were stained with primary and gold-conjugated secondary antibodies on carbon-coated glass. Sections were viewed on a JEM-1400 transmission microscope (JEOL) at 80 kV with an AMT XR111 4k digital camera. For *in vitro* assays, a monolayer of BMECs on transwell inserts was infected with alphavirus at an MOI of 200. After 30 min, culture medium was replaced with fixative buffer (2% PFA and 2.5% glutaraldehyde in 100 mM sodium cacodylate buffer, pH 7.2) and incubated for 1 h at room temperature. Cells were then rinsed with sodium cacodylate buffer and embedded in a thin layer of 2.5% agarose, followed by 1 h of fixation in 1% osmium tetroxide (Polysciences Inc.). After extensive washing with distilled water (dH₂O), cells were stained with 1% aqueous uranyl acetate (Ted Pella Inc., Redding, CA) for 1 h, dehydrated through a series of ethanol concentrations in distilled water, and embedded in Eponate 12 resin (Ted Pella Inc.). Ultrathin sections were generated at 95 nm using an UCT ultramicrotome (Leica Microsystems Inc., Bannockburn, IL) and stained with uranyl acetate and lead citrate. Electron micrographs were obtained using a transmission electron microscope (JEOL 1200 EX; JEOL USA Inc., Peabody, MA) equipped with an AMT 8-megapixel digital camera and AMT Image Capture Engine V602 software (Advanced Microscopy Techniques, Woburn, MA).

Freeze fracture deep etching electron microscopy. Freeze fracture electron microscopy was achieved as described previously (65). Briefly, cultured BMECs were rapidly frozen by abrupt application of the sample against a liquid helium-cooled copper block with a Cryopress freezing machine. Samples were then moved to a liquid nitrogen-cooled Balzers 400 vacuum evaporator, fractured, and etched at -104°C for 2.5 min. For immuno-freeze fracture EM, etched samples were first stained with primary and gold-conjugated secondary antibodies on carbon-coated glass. These samples were then rotary replicated with platinum (~2 nm), deposited from a 20° angle above the horizontal plane, followed by an immediate stabilization film of pure carbon (~10 nm) deposited from an 85° angle. Replicas were floated onto bleach and transferred through multiple rinses of dH₂O before placing on Formvar-coated EM grids. Electron micrographs were obtained using a JEM1400 transmission microscope (JEOL) at 80 kV, equipped with an AMT XR111 4k digital camera.

Statistical analysis. Statistical analysis was performed using GraphPad Prism 7 software. A probability value of $P < 0.05$ was considered statistically significant. Statistical values are indicated as follows: *, $P < 0.05$; **, $P < 0.01$; ***, $P < 0.001$.

SUPPLEMENTAL MATERIAL

Supplemental material is available online only.

FIG S1, TIF file, 0.7 MB.

FIG S2, TIF file, 2.5 MB.

FIG S3, TIF file, 0.9 MB.

FIG S4, TIF file, 9.7 MB.

FIG S5, TIF file, 7.3 MB.

FIG S6, TIF file, 0.6 MB.

FIG S7, TIF file, 0.1 MB.

ACKNOWLEDGMENTS

This work was supported by Defense Threat Reduction Agency (DTRA) grants HDTRA1-15-1-0032 (R.S.K.) and HDTRA1-15-1-0047 (W.B.K.) and NIH grants U19 AI083019, R01 NS052632, and R01 AI101400 (R.S.K.).

We have no conflicting interests to declare.

REFERENCES

- Liebner S, Dijkhuizen RM, Reiss Y, Plate KH, Agalliu D, Constantin G. 2018. Functional morphology of the blood-brain barrier in health and disease. *Acta Neuropathol* 135:311–336. <https://doi.org/10.1007/s00401-018-1815-1>.
- Dando SJ, Mackay-Sim A, Norton R, Currie BJ, John JAS, Ekberg JAK, Batzloff M, Ulett GC, Beacham IR. 2014. Pathogens penetrating the central nervous system: infection pathways and the cellular and molecular mechanisms of invasion. *Clin Microbiol Rev* 27:691–726. <https://doi.org/10.1128/CMR.00118-13>.
- Lachenmaier SM, Deli MA, Meissner M, Liesenfeld O. 2011. Intracellular transport of *Toxoplasma gondii* through the blood-brain barrier. *J Neuroimmunol* 232:119–130. <https://doi.org/10.1016/j.jneuroim.2010.10.029>.
- Zhao Y-L, Song J-N, Zhang M. 2014. Role of caveolin-1 in the biology of the blood-brain barrier. *Rev Neurosci* 25:247–254. <https://doi.org/10.1515/revneuro-2013-0039>.
- Andreone BJ, Chow BW, Tata A, Lacoste B, Ben-Zvi A, Bullock K, Deik AA, Ginty DD, Clish CB, Gu C. 2017. Blood-brain barrier permeability is regulated by lipid transport-dependent suppression of caveolae-mediated transcytosis. *Neuron* 94:581–594.e5. <https://doi.org/10.1016/j.neuron.2017.03.043>.
- Preston JE, Joan Abbott N, Begley DJ. 2014. Transcytosis of macromolecules at the blood-brain barrier. *Adv Pharmacol* 71:147–163. <https://doi.org/10.1016/bs.apha.2014.06.001>.
- Coyne CB, Bozym R, Morosky SA, Hanna SL, Mukherjee A, Tudor M, Kim KS, Cherry S. 2011. Comparative RNAi screening reveals host factors involved in enterovirus infection of polarized endothelial monolayers. *Cell Host Microbe* 9:70–82. <https://doi.org/10.1016/j.chom.2011.01.001>.
- Van den Broeke C, Jacob T, Favoreel HW. 2014. Rho'ing in and out of cells. *Small GTPases* 5:e28318. <https://doi.org/10.4161/sgtp.28318>.
- Persidsky Y, Heilman D, Haorah J, Zelivyanskaya M, Persidsky R, Weber GA, Shimokawa H, Kaibuchi K, Ikezu T. 2006. Rho-mediated regulation of tight junctions during monocyte migration across the blood-brain barrier in HIV-1 encephalitis (HIVE). *Blood* 107:4770–4780. <https://doi.org/10.1182/blood-2005-11-4721>.
- Afonso PV, Ozden S, Cumont M-C, Seilhean D, Cartier L, Rezaie P, Mason S, Lambert S, Huerre M, Gessain A, Couraud P-O, Pique C, Ceccaldi P-E, Romero IA. 2008. Alteration of blood-brain barrier integrity by retroviral infection. *PLoS Pathog* 4:e1000205. <https://doi.org/10.1371/journal.ppat.1000205>.
- Daniels BP, Holman DW, Cruz-Orengo L, Jujjavarapu H, Durrant DM, Klein RS. 2014. Viral pathogen-associated molecular patterns regulate blood-brain barrier integrity via competing innate cytokine signals. *mBio* 5:e01476-14. <https://doi.org/10.1128/mBio.01476-14>.
- Miner JJ, Daniels BP, Shrestha B, Proenca-Modena JL, Lew ED, Lazear HM, Gorman MJ, Lemke G, Klein RS, Diamond MS. 2015. The TAM receptor Mertk protects against neuroinvasive viral infection by maintaining blood-brain barrier integrity. *Nat Med* 21:1464–1472. <https://doi.org/10.1038/nm.3974>.
- Phillips AT, Rico AB, Stauff CB, Hammond SL, Aboellail TA, Tjalkens RB, Olson KE. 2016. Entry sites of Venezuelan and western equine encephalitis viruses in the mouse central nervous system following peripheral infection. *J Virol* 90:5785–5796. <https://doi.org/10.1128/JVI.03219-15>.
- Vogel P, Kell WM, Fritz DL, Parker MD, Schoepp RJ. 2005. Early events in the pathogenesis of eastern equine encephalitis virus in mice. *Am J Pathol* 166:159–171. [https://doi.org/10.1016/S0002-9440\(10\)62241-9](https://doi.org/10.1016/S0002-9440(10)62241-9).
- Ronca SE, Dineley KT, Paessler S. 2016. Neurological sequelae resulting from encephalitic alphavirus infection. *Front Microbiol* 7:959. <https://doi.org/10.3389/fmicb.2016.00959>.
- Zacks MA, Paessler S. 2010. Encephalitic alphaviruses. *Vet Microbiol* 140:281–286. <https://doi.org/10.1016/j.vetmic.2009.08.023>.
- Charles PC, Walters E, Margolis F, Johnston RE. 1995. Mechanism of neuroinvasion of Venezuelan equine encephalitis virus in the mouse. *Virology* 208:662–671. <https://doi.org/10.1006/viro.1995.1197>.
- Schäfer A, Brooke CB, Whitmore AC, Johnston RE. 2011. The role of the blood-brain barrier during Venezuelan equine encephalitis virus infection. *J Virol* 85:10682–10690. <https://doi.org/10.1128/JVI.05032-11>.
- Wang E, Barrera R, Boshell J, Ferro C, Freier JE, Navarro JC, Salas R, Vasquez C, Weaver SC. 1999. Genetic and phenotypic changes accompanying the emergence of epizootic subtype IC Venezuelan equine encephalitis viruses from an enzootic subtype ID progenitor. *J Virol* 73:4266–4271. <https://doi.org/10.1128/JVI.73.5.4266-4271.1999>.
- Mossel EC, Ledermann JP, Phillips AT, Borland EM, Powers AM, Olson KE. 2013. Molecular determinants of mouse neurovirulence and mosquito infection for Western equine encephalitis virus. *PLoS One* 8:e60427. <https://doi.org/10.1371/journal.pone.0060427>.
- Nitta T, Hata M, Gotoh S, Seo Y, Sasaki H, Hashimoto N, Furuse M, Tsukita S. 2003. Size-selective loosening of the blood-brain barrier in claudin-5-deficient mice. *J Cell Biol* 161:653–660. <https://doi.org/10.1083/jcb.200302070>.
- Gong Y, Yu M, Yang J, Gonzales E, Perez R, Hou M, Tripathi P, Hering-Smith KS, Hamm LL, Hou J. 2014. The Cap1-claudin-4 regulatory pathway is important for renal chloride reabsorption and blood pressure regulation. *Proc Natl Acad Sci U S A* 111:E3766–E3774. <https://doi.org/10.1073/pnas.1406741111>.
- Gardner CL, Burke CW, Tesfay MZ, Glass PJ, Klimstra WB, Ryman KD. 2008. Eastern and Venezuelan equine encephalitis viruses differ in their ability to infect dendritic cells and macrophages: impact of altered cell tropism on pathogenesis. *J Virol* 82:10634–10646. <https://doi.org/10.1128/JVI.01323-08>.
- Zhang R, Hryc CF, Cong Y, Liu X, Jakana J, Gorchakov R, Baker ML, Weaver SC, Chiu W. 2011. 4.4 Å cryo-EM structure of an enveloped alphavirus Venezuelan equine encephalitis virus. *EMBO J* 30:3854–3863. <https://doi.org/10.1038/emboj.2011.261>.
- Kovtun O, Tillu VA, Ariotti N, Parton RG, Collins BM. 2015. Cavin family proteins and the assembly of caveolae. *J Cell Sci* 128:1269–1278. <https://doi.org/10.1242/jcs.167866>.
- Predescu SA, Predescu DN, Malik AB. 2007. Molecular determinants of endothelial transcytosis and their role in endothelial permeability. *Am J Physiol Lung Cell Mol Physiol* 293:L823–L842. <https://doi.org/10.1152/ajplung.00436.2006>.
- Echarri A, Pozo MAD. 2015. Caveolae—mechanosensitive membrane invaginations linked to actin filaments. *J Cell Sci* 128:2747–2758. <https://doi.org/10.1242/jcs.153940>.
- Komarova YA, Kruse K, Mehta D, Malik AB. 2017. Protein interactions at endothelial junctions and signaling mechanisms regulating endothelial permeability. *Circ Res* 120:179–206. <https://doi.org/10.1161/CIRCRESAHA.116.306534>.
- Stockton RA, Shenkar R, Awad IA, Ginsberg MH. 2010. Cerebral cavernous malformations proteins inhibit Rho kinase to stabilize vascular integrity. *J Exp Med* 207:881–896. <https://doi.org/10.1084/jem.20091258>.
- Ferri N, Corsini A, Bottino P, Clerici F, Contini A. 2009. Virtual screening

- approach for the identification of new Rac1 inhibitors. *J Med Chem* 52:4087–4090. <https://doi.org/10.1021/jm8015987>.
31. Gonçalves-Carneiro D, McKeating JA, Bailey D. 2017. The measles virus receptor SLAMF1 can mediate particle endocytosis. *J Virol* 91:e02255-16. <https://doi.org/10.1128/JVI.02255-16>.
 32. Carter GC, Bernstone L, Baskaran D, James W. 2011. HIV-1 infects macrophages by exploiting an endocytic route dependent on dynamin, Rac1 and Pak1. *Virology* 409:234–250. <https://doi.org/10.1016/j.virol.2010.10.018>.
 33. Honnold SP, Mossel EC, Bakken RR, Lind CM, Cohen JW, Eccleston LT, Spurgers KB, Erwin-Cohen R, Glass PJ, Maheshwari RK. 2015. Eastern equine encephalitis virus in mice II: pathogenesis is dependent on route of exposure. *Virology* 481:12–154. <https://doi.org/10.1016/j.virol.2015.05.0385-2>.
 34. Cain MD, Salimi H, Gong Y, Yang L, Hamilton SL, Heffernan JR, Hou J, Miller MJ, Klein RS. 2017. Virus entry and replication in the brain precedes blood-brain barrier disruption during intranasal alphavirus infection. *J Neuroimmunol* 308:118–130. <https://doi.org/10.1016/j.jneuroim.2017.04.008>.
 35. Sharma A, Bhomia M, Honnold SP, Maheshwari RK. 2011. Role of adhesion molecules and inflammation in Venezuelan equine encephalitis virus infected mouse brain. *Virology* 418:197. <https://doi.org/10.1016/j.virol.2011.08.0197>.
 36. Erbar S, Maisner A. 2010. Nipah virus infection and glycoprotein targeting in endothelial cells. *Virology* 407:305. <https://doi.org/10.1016/j.virol.2010.07.035>.
 37. Soilu-Hänninen M, Erälänpää JP, Hukkanen V, Röttä M, Salmi AA, Salonen R. 1994. Semliki Forest virus infects mouse brain endothelial cells and causes blood-brain barrier damage. *J Virol* 68:6291–6298. <https://doi.org/10.1128/JVI.68.10.6291-6298>.
 38. Chhatbar C, Detje CN, Grabski E, Borst K, Spanier J, Ghita L, Elliott DA, Jordão MJ, Mueller N, Sutton J, Prajeeth CK, Gudi V, Klein MA, Prinz M, Bradke F, Stangel M, Kalinke U. 2018. Type I interferon receptor signaling of neurons and astrocytes regulates microglia activation during viral encephalitis. *Cell Rep* 25:118–129.e4. <https://doi.org/10.1016/j.celrep.2018.09.003>.
 39. Nair S, Poddar S, Shimak RM, Diamond MS. 2017. Interferon regulatory factor 1 protects against Chikungunya virus-induced immunopathology by restricting infection in muscle cells. *J Virol* 91:e01419-17. <https://doi.org/10.1128/JVI.01419-17>.
 40. Gardner CL, Yin J, Burke CW, Klimstra WB, Ryman KD. 2009. Type I interferon induction is correlated with attenuation of a South American eastern equine encephalitis virus strain in mice. *Virology* 390:338–347. <https://doi.org/10.1016/j.virol.2009.05.030>.
 41. Chanthick C, Suttiheptumrong A, Rawarak N, Pattanakitsakul S. 2018. Transcytosis involvement in transport system and endothelial permeability of vascular leakage during dengue virus infection. *Viruses* 10:E69. <https://doi.org/10.3390/v10020069>.
 42. Chanthick C, Kanlaya R, Kiatbumrung R, Pattanakitsakul S, Thongboonkerd V. 2016. Caveolae-mediated albumin transcytosis is enhanced in dengue-infected human endothelial cells: a model of vascular leakage in dengue hemorrhagic fever. *Sci Rep* 6:31855. <https://doi.org/10.1038/srep31855>.
 43. Brown RS, Wan JJ, Kielian M. 2018. The alphavirus exit pathway: what we know and what we wish we knew. *Viruses* 10:E89. <https://doi.org/10.3390/v10020089>.
 44. Laakkonen P, Auvinen P, Kujala P, Kääriäinen L. 1998. Alphavirus replicase protein NSP1 induces filopodia and rearrangement of actin filaments. *J Virol* 72:10265–10269. <https://doi.org/10.1128/JVI.72.12.10265-10269.1998>.
 45. Ahola T, Kujala P, Tuittila M, Blom T, Laakkonen P, Hinkkanen A, Auvinen P. 2000. Effects of palmitoylation of replicase protein nsP1 on alphavirus infection. *J Virol* 74:6725–6733. <https://doi.org/10.1128/jvi.74.15.6725-6733.2000>.
 46. Knowland D, Arac A, Sekiguchi KJ, Hsu M, Lutz SE, Perrino J, Steinberg GK, Barres BA, Nimmerjahn A, Agalliu D. 2014. Stepwise recruitment of transcellular and paracellular pathways underlies blood-brain barrier breakdown in stroke. *Neuron* 82:603–617. <https://doi.org/10.1016/j.neuron.2014.03.003>.
 47. Castejón OJ. 1980. Electron microscopic study of capillary wall in human cerebral edema. *J Neuropathol Exp Neurol* 39:296–328. <https://doi.org/10.1097/00005072-198005000-00006>.
 48. Claudio L, Raine CS, Brosnan CF. 1995. Evidence of persistent blood-brain barrier abnormalities in chronic-progressive multiple sclerosis. *Acta Neuropathol* 90:228–238. <https://doi.org/10.1007/bf00296505>.
 49. Long M, Huang S-H, Wu C-H, Shackelford GM, Jong A. 2012. Lipid raft/caveolae signaling is required for *Cryptococcus neoformans* invasion into human brain microvascular endothelial cells. *J Biomed Sci* 19:19. <https://doi.org/10.1186/1423-0127-19-19>.
 50. Kiss AL, Botos E. 2009. Endocytosis via caveolae: alternative pathway with distinct cellular compartments to avoid lysosomal degradation? *J Cell Mol Med* 13:1228–1237. <https://doi.org/10.1111/j.1582-4934.2009.00754.x>.
 51. Tugizov SM, Herrera R, Palefsky JM. 2013. Epstein-Barr virus transcytosis through polarized oral epithelial cells. *J Virol* 87:8179–8194. <https://doi.org/10.1128/JVI.00443-13>.
 52. Kinlock BL, Wang Y, Turner TM, Wang C, Liu B. 2014. Transcytosis of HIV-1 through vaginal epithelial cells is dependent on trafficking to the endocytic recycling pathway. *PLoS One* 9:e96760. <https://doi.org/10.1371/journal.pone.0096760>.
 53. Papa MP, Meuren LM, Coelho SVA, Lucas CGO, Mustafá YM, Lemos Matassoli F, Silveira PP, Frost PS, Pezzuto P, Ribeiro MR, Tanuri A, Nogueira ML, Campanati L, Bozza MT, Paula Neto HA, Pimentel-Coelho PM, Figueiredo CP, de Aguiar RS, de Arruda LB. 2017. Zika virus infects, activates, and crosses brain microvascular endothelial cells, without barrier disruption. *Front Microbiol* 8:2557. <https://doi.org/10.3389/fmicb.2017.02557>.
 54. Chaudhary N, Gomez GA, Howes MT, Lo HP, McMahon K-A, Rae JA, Schieber NL, Hill MM, Gaus K, Yap AS, Parton RG. 2014. Endocytic crosstalk: caveolins, caveolins, and caveolae regulate clathrin-independent endocytosis. *PLoS Biol* 12:e1001832. <https://doi.org/10.1371/journal.pbio.1001832>.
 55. Favorel HW, Enquist LW, Feierbach B. 2007. Actin and Rho GTPases in herpesvirus biology. *Trends Microbiol* 15:426–433. <https://doi.org/10.1016/j.tim.2007.08.003>.
 56. Locker JK, Kuehn A, Schleich S, Rutter G, Hohenberg H, Wepf R, Griffiths G. 2000. Entry of the two infectious forms of vaccinia virus at the plasma membrane is signaling-dependent for the IMV but not the EEV. *Mol Biol Cell* 11:2497–2511. <https://doi.org/10.1091/mbc.11.7.2497>.
 57. Schowalter RM, Wurth MA, Aguilar HC, Lee B, Moncan LM, McCann RO, Dutch RE. 2006. Rho GTPase activity modulates paramyxovirus fusion protein-mediated cell–cell fusion. *Virology* 350:323–334. <https://doi.org/10.1016/j.virol.2006.01.033>.
 58. Drewry LL, Jones NG, Wang Q, Onken MD, Miller MJ, Sibley LD. 2019. The secreted kinase ROP17 promotes *Toxoplasma gondii* dissemination by hijacking monocyte tissue migration. *Nat Microbiol* 4:1951–1963. <https://doi.org/10.1038/s41564-019-0504-8>.
 59. Agarwal V, Hammerschmidt S. 2009. Cdc42 and the phosphatidylinositol 3-kinase-Akt pathway are essential for PspC-mediated internalization of pneumococci by respiratory epithelial cells. *J Biol Chem* 284:19427–19436. <https://doi.org/10.1074/jbc.M109.003442>.
 60. Bhalla N, Sun C, Matthew Lam LK, Gardner CL, Ryman KD, Klimstra WB. 2016. Host translation shutoff mediated by non-structural protein 2 is a critical factor in the antiviral state resistance of Venezuelan equine encephalitis virus. *Virology* 496:147–165. <https://doi.org/10.1016/j.virol.2016.06.005>.
 61. Blakely PK, Delekta PC, Miller DJ, Irani DN. 2015. Manipulation of host factors optimizes the pathogenesis of western equine encephalitis virus infections in mice for antiviral drug development. *J Neurovirol* 21:43–55. <https://doi.org/10.1007/s13365-014-0297-8>.
 62. Boroujerdi A, Tigges U, Welsch-Alves JV, Milner R. 2014. Isolation and culture of primary pericytes from mouse brain. *Methods Mol Biol* 1135:383–392. https://doi.org/10.1007/978-1-4939-0320-7_31.
 63. Weksler BB, Subileau EA, Perrière N, Charneau P, Holloway K, Leveque M, Tricoire-Leignel H, Nicotra A, Bourdoulous S, Turowski P, Male DK, Roux F, Greenwood J, Romero IA, Couraud PO. 2005. Blood-brain barrier-specific properties of a human adult brain endothelial cell line. *FASEB J* 19:1872–1874. <https://doi.org/10.1096/fj.04-3458fj>.
 64. Sun C, Gardner CL, Watson AM, Ryman KD, Klimstra WB. 2014. Stable, high-level expression of reporter proteins from improved alphavirus expression vectors to track replication and dissemination during encephalitic and arthritogenic disease. *J Virol* 88:2035–2046. <https://doi.org/10.1128/JVI.02990-13>.
 65. Heuser JE, Kirschner MW. 1980. Filament organization revealed in platinum replicas of freeze-dried cytoskeletons. *J Cell Biol* 86:212–234. <https://doi.org/10.1083/jcb.86.1.212>.